

ISASI 2019 - Investigation of the in-flight failure of the Stratos III Sounding Rocket

Rolf Wubben, *Lead Investigator*

Eoghan Gilleran, *General Investigator*

Krijn de Kievit, *General Investigator*

Bart Kevers, *Structural Analysis*

Maurits van Heijningen, *Data Analysis*

Martin Christiaan Olde, *RCA Methodology*

Delft Aerospace Rocket Engineering, Stevinweg 1 2628 CN Delft, South Holland, The Netherlands

The Stratos III sounding rocket is a rocket developed by students from Delft Aerospace Rocket Engineering (DARE) at Delft University of Technology. It is the third generation of the Stratos rocket and was intended to break the European student altitude record of 33.5 km. However, 22.12 seconds into the flight of Stratos III an anomaly occurred, resulting in the loss of the vehicle. At this time, the rocket was travelling at approximately Mach 3 at an altitude of 10 km. An investigation was performed by the students of DARE with the help of Delft University of Technology personnel. The purpose of this report is to show how the investigation was performed, what the results are, how future anomalies can be prevented and how future investigations can be improved.

After performing a root cause analysis (RCA) it was determined that inertial roll coupling was the main cause of the Stratos III anomaly. This could be concluded from data provided by on-board inertial measurement units (IMUs) as well as ground radar and Doppler data. This data shows divergence of the sideslip angles of the rocket during flight, until the limit values are reached at the disintegration event. Inertial roll coupling is a complex phenomenon that can be caused by a plethora of different factors, such as the large length to diameter ratio of the rocket or flexibility and misalignment of the rocket body, resulting in both a large effective thrust misalignment as well as an induced aerodynamic pitching moment. The latter is definitely a factor to improve in the Stratos IV rocket. Moreover, balancing of the centre of gravity and changing the static margin of the rocket can be used to prevent future anomalies. Furthermore, to assist in the conduction of future investigations, not only should the rocket record more data during flight and stream it back to the ground, but also more information about the rocket, such as structural stiffness and section masses, should be recorded before lift-off. Lastly, more attention should be paid to integrated testing of full systems, as a lack of this caused most of the problems pre-launch for the launch crew, as well as post-launch for the investigation team.

Nomenclature

Acronyms

PCB	Printed Circuit Board	FTS	Flight Termination System
RCA	Root Cause Analysis	IMU	Inertial Measurement Unit
CEDEA	Centro de Ensayos de El Arenosillo	INTA	Instituto Nacional de Técnica Aeroespacial
cg	centre of gravity	ISA	International Standard Atmosphere
DARE	Delft Aerospace Rocket Engineering	L/D	Length to Diameter ratio
FTR	Flight Termination Receiver	SL	Sea Level

Greek Symbols

α	Angle of attack	[deg]
α_{sr}	Effective static trim angle of attack	[deg]
Δcg	Lateral cg offset	[m]
δ	Effective fin cant angle	[deg]
τ	Effective thrust asymmetry angle	[deg]
γ	Isentropic expansion factor	[-]

Roman Symbols

a	Speed of sound	[ms ⁻¹]
c_{mo}	Moment coefficient at $\alpha = 0$	[m]
d	Rocket diameter	[m]
M	Mach number	[-]
R	Specific gas constant	[Jkg ⁻¹ K ⁻¹]
T	Air temperature	[K]
x_{cg}	Centre of gravity location	[m]
x_{cp}	Centre of pressure location	[m]

I. Introduction

Around the world a large number of student groups are participating in the new space race. The goal: To be the first student team to reach the Kármán line with a rocket, fully developed and built by students. One of these teams is Delft Aerospace Rocket Engineering (DARE) which, with the Stratos I, Stratos II+ and Stratos III rockets has attempted to break the (European) student altitude record and aim to be the first student team in the world to reach space. DARE's 150 students independently organise many small launches on a yearly basis. In addition, DARE is one of the only student societies in the world that has launched rockets from professional international launch sites.

Stratos III is an 8.2 meters long single stage hybrid sounding rocket that includes several scientific payloads. The Stratos III rocket was launched at 01:16:25 UTC on the 26th of July 2018 from the Spanish launchsite Centro de Ensayos de El Arenosillo (CEDEA) operated by the Instituto Nacional de Técnica Aeroespacial (INTA). 22.12 seconds into the flight, at an altitude of 10 km the rocket disintegrated, failing to reach the intended altitude of approximately 68 km.

This in-flight disintegration afforded the students of DARE a unique opportunity to conduct an investigation into such an anomaly. The purpose of this paper is to provide an overview of the investigation into the in-flight anomaly, discussing the implemented methodology and provide an overview of the conclusions, both of the investigation itself, as well as how such an investigation may be conducted and better prepared in the future. With work on a new space shot attempt, Stratos IV, underway, a swift investigation was necessary for the team to improve the design and regain confidence in future launches. Moreover, in the event that a similar loss of vehicle event was to occur in a future flight, insights gained from this investigation may be used to allow for a more complete and confident result from the following investigation.

The paper is structured as follows: section II presents an overview of the Stratos III sounding rocket's technical parameters, section III discusses the data sources used for this investigation, and describes what can be seen in the acquired data, section IV presents the methods used during the investigation, section V describes the implementation of this methodology and the cause that is found, section VI further analyses this root cause, and finally section VII presents the conclusions of the investigation and recommendations regarding improving the preparation for, and conduction of future investigations. Appendix A describes the implementation of several technical recommendations in the Stratos IV rocket.

II. Vehicle Analysis

The Stratos III rocket was designed to break the European altitude record at 32.3 km set in 2016. For this, new and lightweight composite structures were introduced compared to the aluminium structure of Stratos II+ and a new engine was developed. The engine is a hybrid rocket engine, the most powerful ever developed by students, with a peak thrust of 26 kN. It uses liquid nitrous oxide (N_2O) as the oxidiser, and a mixture of sorbitol, paraffin and aluminium powder as the fuel in the solid fuel grain.

Next to the engine, the rocket consists of 5 additional sections, shown in Figure 1. From top to bottom these are:

1. Nosecone: containing all the important flight electronics that control the flight systems as well as the black boxes that store all of the flight data that is recorded. This includes static pressure and XSens IMU data, which is very important to reconstruct the trajectory after recovery. Moreover, the telemetry and video antennas are located here, that stream down important information to the ground stations at 869 MHz for telemetry and 2.4 GHz for video. The outer shell is made out of glass fibre since it is required to be radio-transparent to the telemetry frequencies.
2. Recovery Bay: containing both of the parachutes for recovery. A drogue parachute is deployed by pressurising its container with gaseous carbon dioxide. A spring deployed main parachute is used to slow down the capsule to a landing velocity of 15 ms^{-1} . The rocket separates at the bottom of this section at apogee. Only the capsule is recovered.
3. Tank: containing 174.1 kg of nitrous oxide. The tank is made up of a 1.5 mm thick aluminium liner that is overwrapped with carbon fibre to hold the nitrous oxide at 60 bars. The outer shell is made of carbon fibre prepreg.
4. Engine Bay: containing all of the feed system that is required to guide the nitrous oxide from the tank to the engine. 6 kgs^{-1} of nitrous oxide flows through this feed system. All the engine control electronics are located in this section, as well as the flight termination system, which uses a detonation cord to break up the main load carrying structure of the engine bay when a termination signal is sent. The main structure consists of 5 carbon fibre longerons, positioned longitudinally with respect to the rocket's long axis, glued to interface rings at the top and bottom.
5. Fincan: an aerodynamic cover that slides over the engine and engine bay sections to which the fins are attached. This aerodynamic cover is needed because the outer diameter of the tank and the engine are different (278 and 260 respectively). The fincan is made of carbon fibre. The fins itself are sandwich structures consisting of a aluminium honeycomb core and carbon fibre skins. The leading and trailing edges are made out of pertinax.

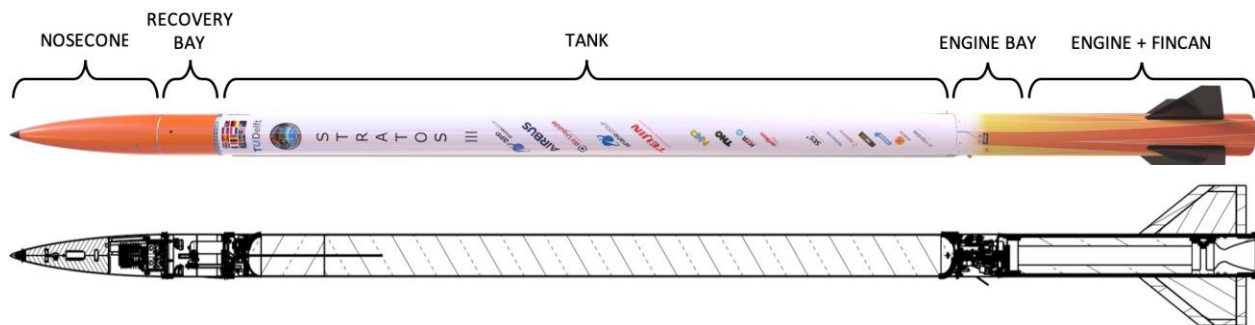


Figure 1: The sections of the Stratos III rocket on the outside and on the cross section

Figure 2 shows the reference frame used for the Stratos III rocket, the body-fixed frame. This is the reference frame that will be used for the rocket throughout this report. The second frame used is the world-fixed frame, which is an inertial frame with the origin at the launch location, the X axis pointing North, the Y axis pointing West and the Z axis completing the orthogonal right-handed coordinate frame.

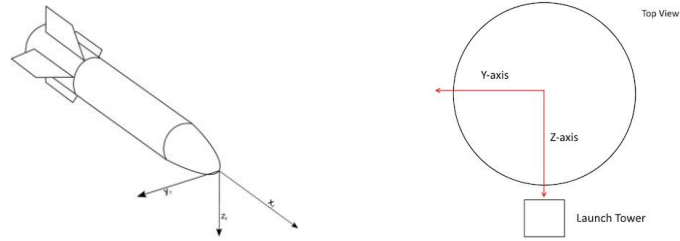


Figure 2: Body frame of the Stratos III rocket. Isometric and top view

Table 1 shows what interfaces were used between the different sections, Table 2 shows the main parameters of the rocket, and Table 3 gives an overview of the sensors on board Stratos III.

Table 1: Overview of Mechanical interfaces

Part 1	Part 2	Interface Description
Nose Cone	Recovery Bay	Bolted connection using 12 M4 radial bolts with aluminium 7075-T6 coupler pieces on both the nose cone and the recovery bay. These aluminium parts are glued into the composite shells of the nose cone and the recovery bay
Recovery Bay	Oxidiser Tank	Stratos III separation system. This system uses a clamp band system where a spring steel band with a v-shaped groove is used to clamp the interfacing parts together. These clamped parts are made out of aluminium 7075-T6, and are glued to the composite shell of the upper skirt on the tank and the recovery bay
Oxidiser Tank	Engine Bay	10 axial M8 bolts are used to attach the flat faces of the oxidiser tank lower skirt (creating a flat interface instead of the hemispherical interface of the tank bulkhead) and the upper bulkhead of the engine bay. Both interfaces are made of aluminium 7075-T6. The carbon fibre engine bay longerons are glued to the engine bay upper bulkhead.
Engine Bay	Engine	10 axial M8 bolts are used to attach the flat faces of the lower bulkhead of the engine bay and the injector manifold in the engine. Both interfaces are made of aluminium 7075-T6. The injector manifold is attached to the aluminium 6060-T6 engine casing by means of 30 radial M8 bolts.

Table 2: Main parameters of Stratos III

Parameter	Value	Unit
Total Wet Mass	343.7	kg
Total Dry Mass	117.6	kg
Length	8.2	m
Main Body Diameter	0.278	m
Number of stages	1	-
Peak Thrust (SL)	26	kN
Average Thrust (SL)	15	kN
Burn Time	37	sec
Total Impulse	380	kNs
Total Fuel Mass	52	kg
Total Oxidizer Mass	174.1	kg

Table 3: Stratos III on-board sensors

Sensor	Amount	Description
Xsens IMU	2	MTI-100-2A8G0
GPS	2	Unlocked Septentrio AsteRx-m
Ambient pressure sensor	2	NXP MPL3115A2 chip
High pressure sensor	2	IFM PT5402, used to measure pressure in the tank and the combustion chamber.
Cameras	4	1 downward facing and 3 radial action cameras. The radial cameras cover 120° each such that a 360° image can be created.

III. Failure Description

Before any in-depth analysis can be conducted, the data upon which this analysis will be based was first gathered and organised. This chapter will present these data sources as well as commenting on the initial conclusions that can be drawn from this data. This data is then further analysed and interpreted in section IV and section V.

A. Data Sources

The data sources included in the investigation of the Stratos III in-flight anomaly were ground based meteorological information, ground based radar tracking of the vehicle and three parts of the post anomaly debris, ground based Doppler shift tracking of the vehicle and the resultant debris, both infra-red and optical footage of the vehicle taken from the ground, as well as one on board data source, being two XSens Inertial Measurement Units (IMUs) as mentioned in Table 3.

Before each launch attempt the practise is to release a weather balloon with a suite of meteorological sensors. Due to the delay in launching Stratos III the last weather balloon release occurred 10 hours before the launch. Thus, there is a possibility that weather conditions varied, yet the simulations conducted to determine the rockets flight path used these wind speed, direction, temperature, humidity and pressure profiles. The radar installation of 1 MW output power present at CEDEA tracked the vehicle up to the anomaly, and then tracks three pieces of debris for 12 seconds, before losing lock and then following one piece of debris all the way to the ground. This data was provided to the investigation team by INTA in coordinate locations of these objects with a 0.02 s time step. From this radar data, INTA personnel identified three distinct events:

Table 4: Time of three distinct events given in UTC (Coordinated Universal Time).

Event	Time (UTC)
TAKE OFF	01:16:25.260
EXPLOSION 1	01:16:47.240
EXPLOSION 2	01:16:47.380

The coordinates from the radar installation were used to plot the location of the various objects throughout time when viewed different perspectives, as well as plotting these debris locations versus time. In addition, the velocity of these objects may be inferred from the "location versus time" plots. In addition to the standard 2D plots supplied by INTA, exemplified in Figure 3a, a number of 3D plots were generated, such as Figure 3b, that allowed the trajectory of the vehicle to be visualised in addition to the velocity being illustrated with a colour profile. This is particularly useful in visualising the trajectory of the debris post anomaly, but also how the debris decelerated and the direction in which they decelerated. The Doppler shift measurements illustrate the velocity of different objects in the instruments field of view. This instrument gives a clear view of when the various break up events occur as each appearance of a new object and its subsequent deceleration is very visually evident as seen in Figure 3c.

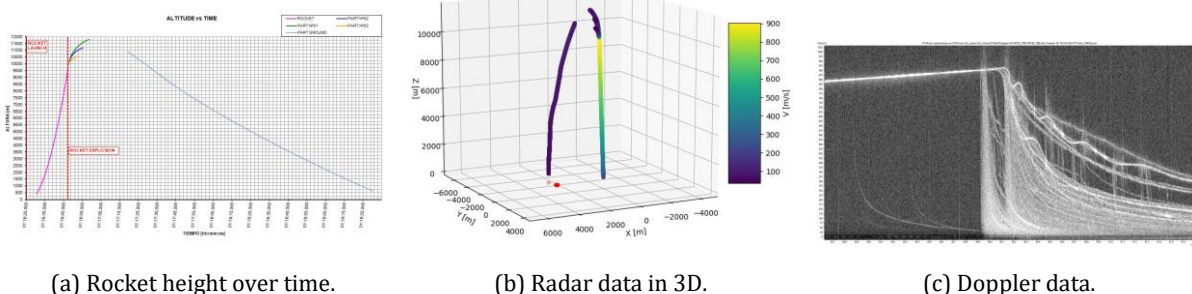


Figure 3: Plots of the radar and Doppler data.

The optical tracking footage, Figure 4c and Figure 4d, does not provide much insight beyond the moment of the disintegration, when the thrust plume disappears and some different debris is lit up spreading out. The infra-red footage, Figure 4a and Figure 4b, however was much more useful in observing the flight. The exhaust plume dominates the footage, but this plume also clearly illustrates the motion the vehicle is undergoing as it almost traces out the trajectory. Post anomaly the debris falling away from the vehicle can be seen, however the perspective of the footage makes it difficult to judge the direction in which the debris flies. In this manner the footage provides more of a visual qualitative source than specifically quantitative information. The Doppler plot that was generated from the footage together with the radar data of the flight is a lot more insightful. Here, two distinctly separate events are visible with 140ms offset from each other. In between the two, some large component keeps accelerating at the same rate as before.



(a) IR footage w/ exhaust trail showing trajectory (b) IR footage showing debris dispersing post anomaly (c) Optical footage pre anomaly (d) Optical footage of debris post anomaly

Figure 4: Frames from IR and optical cameras pre and post anomaly

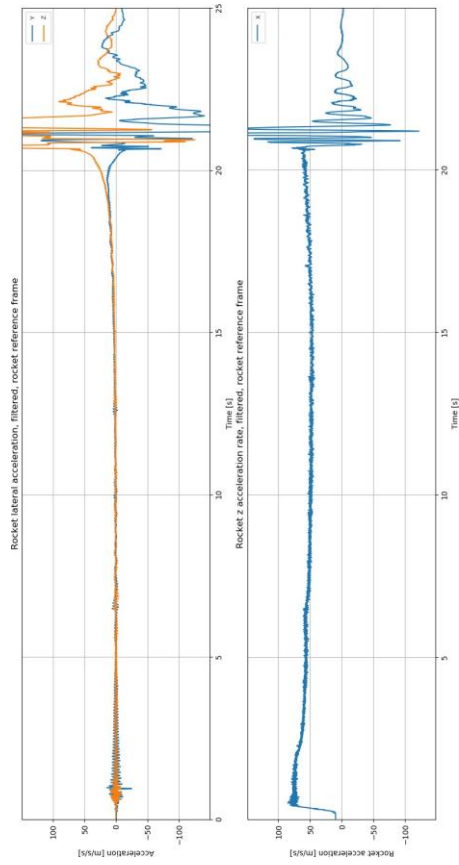
The single usable on-board data source was an XSens IMU, of which there were two placed in the rocket. They were measuring acceleration and rotation rates in all three axes. This data was retrieved from SD cards placed on the PCBs of the flight computer which had stored the data. This data was not retrievable from the on-board black boxes as the data was not successfully written to these SD cards during the flight. Again, this data was plotted in 2D form, with the various parameters depicted versus time.

In the first plot, Figure 5a, the accelerations of the rocket in the rocket reference frame are shown. These accelerations are directly taken from the sensor, with no post-processing done apart from filtering. Lateral accelerations are very low throughout the initial part of the flight, apart from some vibrations around launch. From 12 seconds onward the lateral accelerations start to slowly diverge resulting in exponential divergence just before the anomaly. The longitudinal acceleration spikes at around 8g and remain fairly constant throughout the flight right up and until the anomaly occurs.

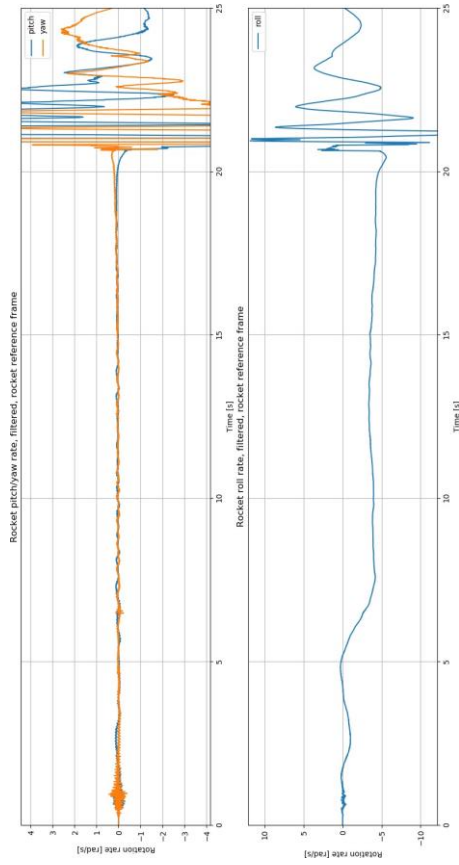
Figure 5b shows the rotation rates of the rocket around its three axes. Again, apart from filtering, these needed no additional conversion. Like the lateral accelerations, the rotation rate in pitch and yaw starts to visibly diverge from 0 after 12 seconds into the flight. Again, just before the anomaly, the values start to increase exponentially.

Figure 5c shows the rocket's sideslip in both lateral directions. The sideslip angle of a rocket is defined as the angle between the rocket's current orientation and its velocity vector. Both these vectors were found by integrating the accelerations and rotation rates measured by the two on board IMUs, after which the angles could easily be determined. Data is limited from one second after ignition to 20.5 seconds after ignition to make sure the plot remains legible. The darkest red point represents the earliest moments of flight. It then gradually changes to dark blue indicating the moment at which the anomaly occurred. In the initial section of the flight the rocket's sideslip angles seem to variate randomly while drifting of some arbitrary general directions. This, however, starts to take shape in a circle or spiral that progressively becomes more consistent.

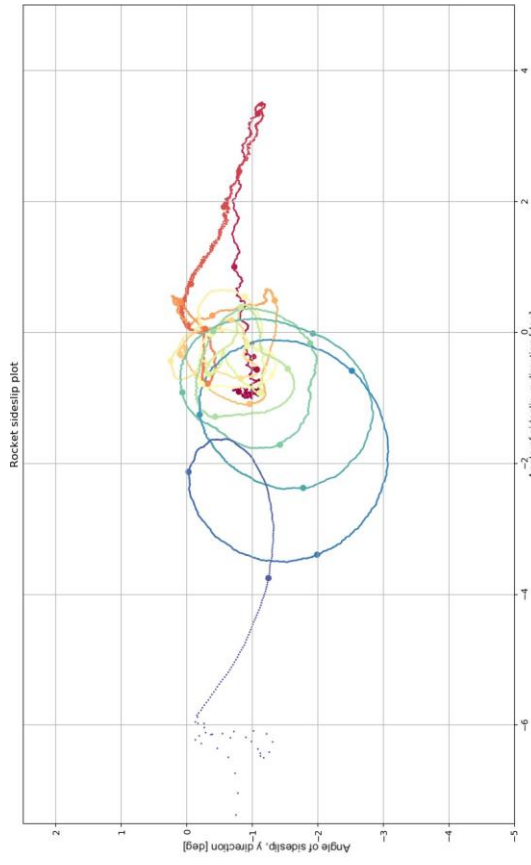
Figure 5d gives the Mach number at which the rocket was travelling. It was determined using the velocity of the rocket together with the temperature of the air, by $a = \sqrt{\gamma RT}$. The temperature was determined using the altitude as an input of the International Standard Atmosphere (ISA) model, calibrated with a temperature of 22 °C at ground level. The Mach number is particularly interesting because it shows when the rocket breaks the sound barrier. Figure 5d shows Mach 1 is reached 7 seconds into the flight. When looking at Figure 5a and Figure 5b, a small spike in the lateral accelerations and rotation rates can be



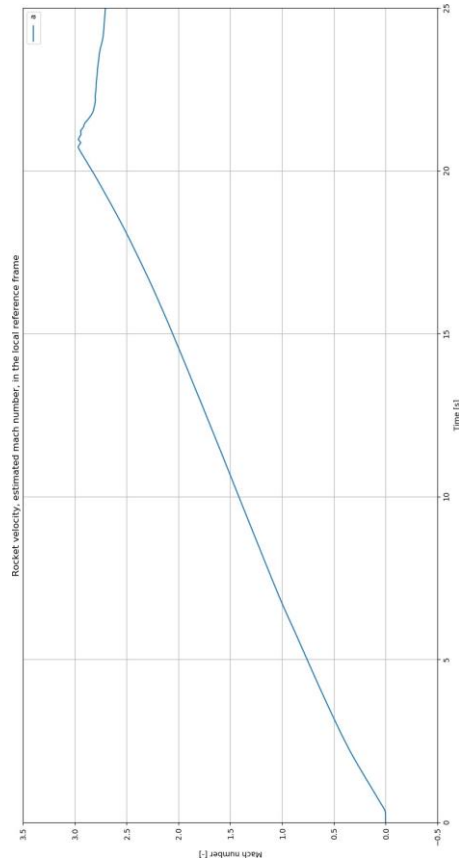
a) Filtered rocket acceleration in the rocket reference frame.



b) Filtered pitch, yaw and roll rates in the rocket reference frame.



c) Rocket sideslip angles α and β



d) Rocket Mach number.

Figure 5: Rocket data

observed at the same time. Furthermore, there is a small decrease of longitudinal acceleration from that point onward. Lastly, the roll rate ceases to increase at this moment for a short period of time but continues increasing steadily directly after.

In order to better visually represent the motion of the vehicle during flight, an animation was constructed. The animation programme can be requested from the authors. It is based on the acceleration and rotational rate data from the two IMUs that were located in the nosecone section. The starting conditions, elevation, azimuth and origin, are synced using the radar data supplied by INTA. The data was retrieved from SD cards that were implemented on the flight computer PCBs, and not from the black boxes. Because of a bug in the software of the black boxes, data was not properly transferred to them, meaning that only very low sample rate data was stored on their SD cards. The investigation team was very lucky to find the flight computer SD cards intact, as otherwise this would have significantly complicated data analysis.

The following three figures attempt to capture the insight the actual video offers in a paper. In Figure 10 an additional attempt is made to intuitively show the motion the rocket is going through, based on the conclusion that has then been reached.

Figure 6a shows the rocket as it was positioned in the launch tower. The darker red, green and blue arrows represent the rocket fixed world coordinate system, with its origin in the physical location of the IMUs in the rocket. The lighter red, green and blue arrows represent the rocket body fixed reference frame. The black line represents the nominal flight path.

Figure 6b represents the initial stable flight of the rocket. The purple line in Figure 6b represents the velocity, and the pink arrow represents the acceleration. Please note that the two rockets in the image result from a small difference between the two IMUs that were on board. Since the data is integrated twice, the error enlarges, resulting in a few meters over the entire flight until the anomaly at an altitude of 10km. The integration error between the sensors starts to add up to a few meters of offset, which is represented by the two rockets flying slightly different trajectories in the animation. A small angle between the acceleration (pink) and velocity (purple) can be observed and a small angle between the nominal flight path and the rocket's longitudinal axis appears.

Figure 6c shows the rockets right before the anomaly. The acceleration vector has diverged sideways significantly. Moreover, a large angle of attack, the angle between the rocket's X-axis and the nominal flight path, can be observed.

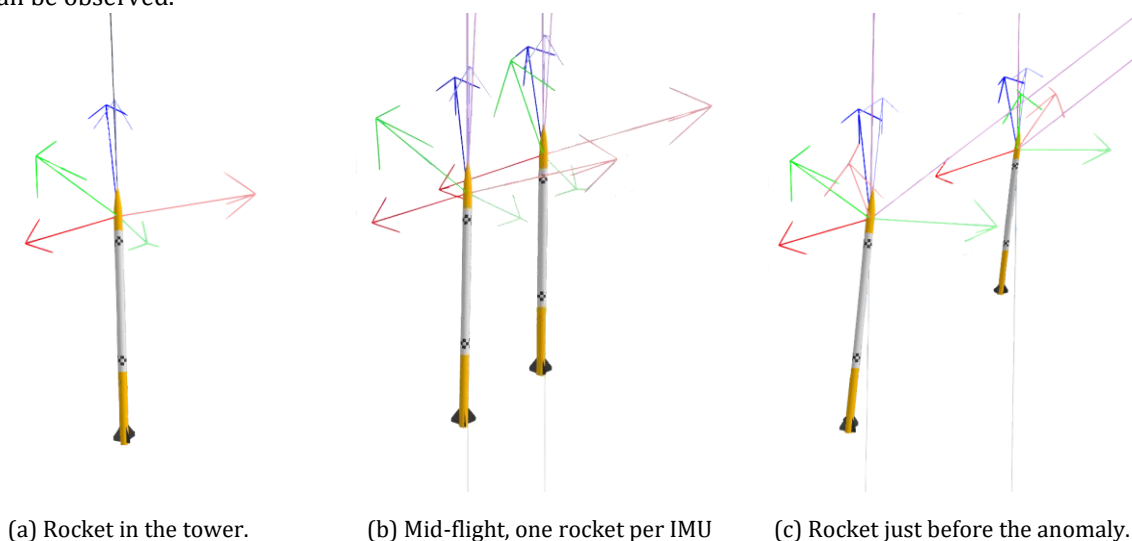


Figure 6: Frames taken from the animation tool, based on the IMU data

Data from the GPS was unreliable as it did not get a proper lock during the flight. Moreover, both the tank pressure as well as the combustion chamber pressure were not recovered due to an error in the hardware interface between the pressure sensors and the flight computer. Additionally, the footage recorded by the on-

board cameras was only stored on these cameras and transmitted through the telemetry downlink, and as the cameras were never recovered, only the low-resolution footage recorded from telemetry was recorded.

B. Debris Inspection and Analysis

After the anomaly, numerous parts of the rocket were tracked to land and then retrieved from restricted military terrain. This included the engine, parts of the fincan (without the fins), half of the engine bay structure, and the flight termination receiver (FTR), the nose cone including the flight computer inside of it, and the drogue feed system. It is interesting to note that the FTR was found close to the nosecone. while the engine bay structure, to which it was attached in flight, was discovered relatively far away, while still being attached to the engine.

The rocket components that were found were photographed and inspected, then taken back to the launch base for further research. Here they were closer inspected, photographed, and analysed by members of DARE. The nosecone, Figure 7a, was seen to be cracked along the glue joint of the two halves, likely from impact forces as the cracked lines ran parallel with the ground. The flight computer had been ejected from the shell as a result of the impact and was badly deformed. The nosecone was broken along its interface with the recovery bay, and no debris was found of the separation system sitting on the lower side of the recovery bay. The drogue parachute feedsystem Figure 7b was seen to have had its connectors sheared out of their ports. The engine bay, Figure 7c, was found with a number of the longitudinal elements (longerons) missing. Those missing had broken off the segment of the aluminium ring they had been attached to, meaning the ring itself had failed before the carbon-aluminium glue joint had. A length of detonation chord was found wrapped around one of the longerons, showing the FTS had not been triggered.

One of the most interesting parts retrieved was the fincan, Figure 7d and Figure 7e. The entire lower half, where the fins had been attached, was missing, having been ripped off during flight. This failure appeared to have been a result of torsional loads. This leads to further investigation of the torsion keys constraining the fincan. It could for instance be that the lack of rigidity of the torsion locks and keys might have contributed to the possible roll-pitch coupling. Or the other way around, where the roll-pitch coupling caused increasing lateral loads on the fins and fincan, until the glued attachment of the torsion keys to the fincan failed. This could have twisted and torn the fincan.



(a) Nosecone Shell



(b) Drogue Parachute Feedsystem



(c) Engine-bay debris



(d) Combustion chamber with upper half of fin can remaining.



(e) Combustion chamber region where fins were attached

Figure 7: Examples of the recovered debris.

Since the fins and bottom part of the fincan were not attached to the rocket anymore, the vehicle did not have any more stabilising surfaces and flipped. This would also line up with the Doppler data in Figure 3c, where the first explosion is the separation of the lower fincan and the rocket, and the second one the full disintegration of the rocket. Structural tests to verify this cause and effect problem were planned but have never been performed.

The engine was squashed from the impact, causing the remaining fuel and nozzle to have cracked, but otherwise it appeared to have burned nominally during the flight, with no evidence of a burn through, a problem that had been observed multiple times during ground tests, being visible.

Additionally, possible root causes of the anomaly like the fin attachment to the fincan, or the arguable stiffness of the engine bay have neither been tested during the time of the investigation.

IV. Methodology

With the collection of all information, as provided in previous sections, and some preliminary data analysis completed, a structured methodology can be set up to determine the cause of the anomaly. Up to this point an attempt was made to prevent significant speculation on the cause of the failure. The methodology followed a three-step approach which was repeated several times as the investigation deepened and new insights were obtained.

1. First an open brainstorm session was held with all stakeholders, including the investigation team, but also with other team members and project partners, during which available data was reviewed and presented. These causes were organised in a fish bone diagram to identify causal relationships, identify root causes that had combined branches. These were informally tested against a 5 why method to discover gaps in causes and their effects.
2. The second step involved the collection of available facts in favour or opposing certain proposed causes. In addition, a selection was made between *open* causes and *unlikely* causes to give some credence to engineering instinct. Based on collected facts the aim was to eliminate, *close* all proposed failure causes and with that establish the final root cause of the failure. This was simplified by trying to disprove certain branches at a high level to reduce the amount of work necessary.
3. The last step involved the collection and analysis of the data, literature and expert opinion to work through the full failure tree. At several occasions the tree was reassessed both on its completeness, but also to determine if any branches or root causes could be conclusively closed. This iteratively led to the conclusions presented in this publication.

A. Investigation Team

The investigation team is primarily composed of DARE members, both those who took part in the Stratos III project and launch campaign, as well as members of the Stratos IV project, with no experience of the Stratos III project or flight campaign. This provides a mix of experience and fresh perspectives to be used during the investigation. Many other DARE members were also relied upon for their recollection of the certain events that happened during launch campaign or as advisers. Additionally, in order to bridge the gap in professional experience in addition to the DARE members, Delft University of Technology personnel were contacted to determine the best method of approach to the investigation.

B. Root Cause Analysis Method

At the start of the investigation, many theories were discussed based on what was being observed in the debris analysis, as well as what members of the team had observed during the course of the flight, and had heard from personnel who had been observing data streams during the flight. These observations were all recorded, and it became evident that a myriad of different possible causes for the anomaly could have resulted in these observations.

The different theories for the cause of the anomaly are organised in Figure 8. This fishbone diagram shows which theories are connected and provides a clear basis to work towards determining the root cause.

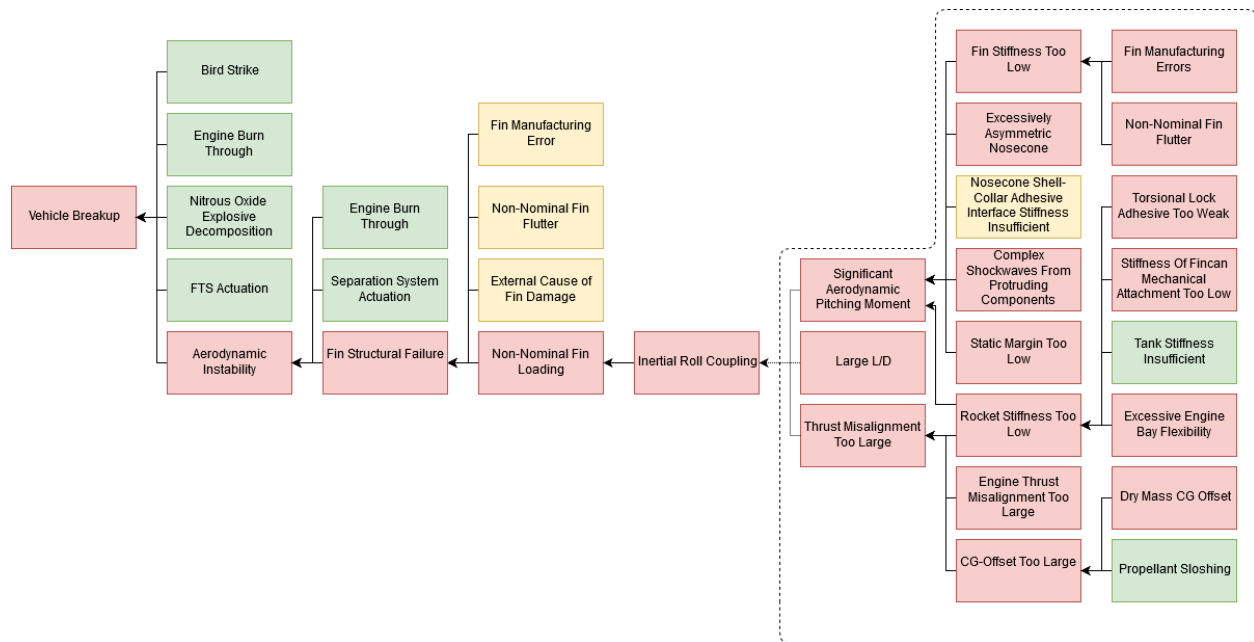


Figure 8: Fishbone diagram of all considered causes for the flight anomaly.

All the suspected causes are analysed separately, after which they are classified as being *closed*, *unlikely* or *open*, depending on their suspected influence on the anomaly. *Closed* means that the cause is discarded as a cause for the in-flight anomaly and corresponds to the colour green. *Unlikely* means that the cause could not be discarded with the available evidence, but that it is not likely that this cause resulted the anomaly. This corresponds to the colour orange. *Open* means that the cause is still a possibility for the anomaly and corresponds to the colour red.

The classification for a suspected cause is determined by extensively describing what the cause entails, then going through the available sources of information to search for both supporting and opposing evidence to determine whether this cause could have resulted in the anomaly or not. Supporting and opposing evidence is then weighed against each other through discussion with the team, and occasionally through further discussion with members who had worked on the relevant system, and classification is determined. Occasionally a calculation or simulation is implemented to test the feasibility of a cause, after which it is assigned its status. If a suspected cause is classified as *closed* then the sub-causes of this branch are also considered closed.

When this process is finalised, only one branch should remain open. The lowest level sub-cause is then considered the most likely root cause for the breakup of Stratos III.

V. Root Cause Analysis

In this section the root cause analysis for the in-flight failure is provided based on the description of the vehicle, description of the failure and the analysis made during the investigation. As mentioned in the previous section several tools were used to aid the analysis. These are summarised below.

A. Fishbone Diagram

A fishbone diagram is used to establish a causal tree of events that could have precipitated the vehicle failure. The fishbone diagram is shown in Figure 9. For brevity the titles were summarised. Compared to Figure 8, note that the methodology is discontinued after inertial roll coupling (5.1.4.1). This was done in order to be able to show one distinct cause of the failure. In this investigation it became apparent that there was no single lowest level root cause to the anomaly. There are instead, multiple contributing factors. All these open sub-causes are treated as a contributing factor to their parent cause: inertial roll coupling.

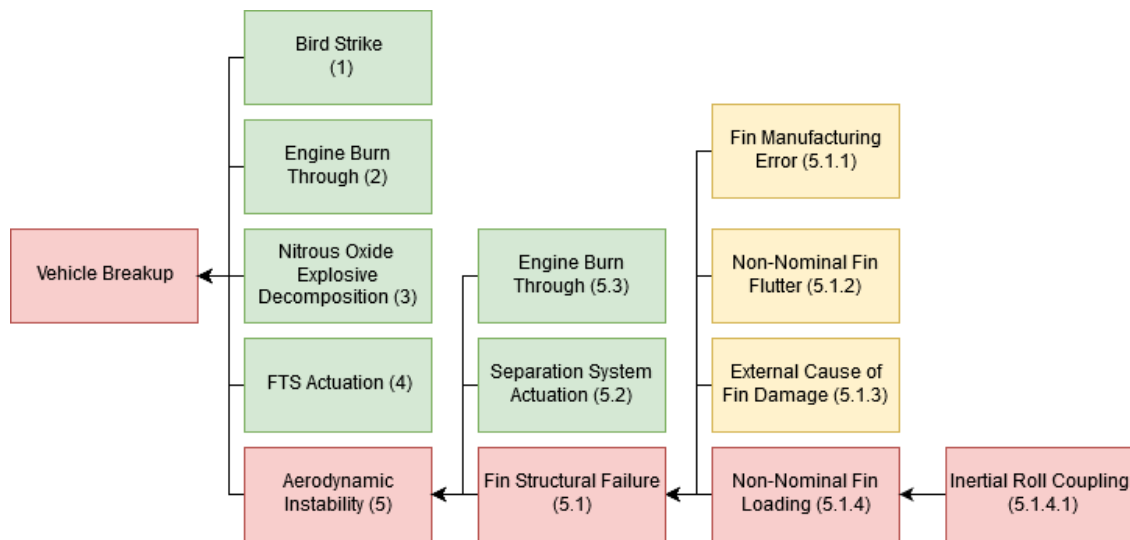


Figure 9: Fishbone diagram with the suspected causes for the rocket failure

B. Classification of suspected causes

The summary table provides all the suspected causes of anomaly considered in the investigation. As explained in section IV, first a description of the cause is provided, after which supporting and opposing evidence determine the status. For all the causes under “Inertial Roll Coupling” the same procedure has been performed. However, as will be elaborated upon in section VI, their exact contribution remained unspecified and unquantified, yielding very little evidence for most of them to give a classification other than open.

Table 5: Summary table of the Stratos III root cause analysis - Part I

No.	Description	Status	Supporting Evidence	Opposing Evidence
1	Bird Strike The rocket impacting a bird would have caused an impulse load into the structure, discontinuing nominal flight.	Closed	Not available.	The chance of a bird strike is very low, no bird debris was observed on the recovered vehicle debris, no birds were observed.
2	Engine Burn Through An engine burn through structurally compromise the combustion chamber, causing the vehicle to structurally fail.	Closed	During ground tests the engine was seen to be prone to burning through.	The recovered engine does not show any sign of burn through.
3	Nitrous Oxide Explosive Decomposition Nitrous oxide is prone to explosive decomposition, which would cause structural failure.	Closed	Nitrous decomposition caused an engine failure during a ground test.	The engine debris does not show any signs of explosive decomposition. This phenomenon is most likely to occur with gaseous nitrous, and the engine was still in the liquid burn phase when the anomaly occurred.
4	FTS Actuation The FTS is intended to structural break up the vehicle in case of a non-nominal flight.	Closed	The rocket appears to have broken in to three distinct pieces, which is the expected outcome of FTS actuation.	Undetonated pieces of detonation cord were found in the engine bay debris.
5	Aerodynamic Instability An aerodynamically unstable vehicle would cause non-nominal structural loads, causing the vehicle to fail structurally.	Open	Not available.	The vehicle begins to diverge in both pitch and yaw rates as well as lateral accelerations moments before it breaks up.
5.1	Fins Structural Failure The fins are responsible for maintaining aerodynamic stability, if they were to fail then the vehicle would become unstable and break up.	Open	The optronics footage shows small pieces of debris flying off of the rocket pre-anomaly. The fin production and attachment was not conducted according the initial plan and was done quite last minute, with uncertainty surrounding the attachment method used.	The IMU data shows that when the small debris separated from the vehicle, it was enduring non-nominal loads. In addition the fin can was seen to have sheared off entirely, meaning it is impossible to observe whether the fins failed individually.

Table 6: Summary table of the Stratos III root cause analysis - Part II

No.	Description	Status	Supporting Evidence	Opposing Evidence
5.1.1	Fin Manufacturing Error The fin attachment was reinforced with a vinyl ester epoxy	Unlikely	The fin can debris showed that the reinforcement patches were ripped cleanly off. It is also known that the reinforcement process was not conducted properly due to improper reinforcement materials being used.	If the attachment failed then the forces on the fin can should lower, meaning the lower half would not have been ripped off.
5.1.2	Non-Nominal Fluttering Fin flutter is the phenomena where fluctuating loads are exerted on fins due to the dynamic pressure being experienced.	Unlikely	Fin flutter is difficult to predict would cause fin structural failure if underestimated.	The fins were designed according to NASA guidelines for flutter sizing.
5.1.3	External Cause of Fin Damage If the fins were to strike a piece of ground equipment (the umbilical or filling apparatus) during launch, then damage may worsen during flight, leading to structural failure.	Unlikely	Not available.	the ground equipment was inspected post launch and no damage was observed. Subsonic flight appeared stable, indicating little or no damage to the fins.
5.1.4	Non-Nominal Loading Non-nominal loading of the fins would cause structural failure resulting in an aerodynamically unstable vehicle.	Open	Not available.	The IMU data shows the vehicle beginning to diverge in both pitch and yaw rates as well as lateral accelerations moments before it breaks up. These rates would certainly induce non- nominal loads on the structure.
5.1.4.1	Inertial-Roll Coupling "Inertial roll coupling is a resonant divergence in pitch or yaw when roll rate equals the lower of the pitch or yaw natural frequencies".[1] This causes the vehicle to become unstable and endure non-nominal structural loading.	Open	Not available.	The IMU data shows the vehicle beginning to diverge in both pitch and yaw rates as well as lateral accelerations moments before it breaks up. Most notably, this divergence starts after a sudden increase in roll rate around the moment the rocket breaks the sound barrier. The roll rate remains constant afterwards. This is consistent with inertial coupling, alternatively named "Spin-Yaw Lock-in"[2]. Once a rocket roll rate reaches this critical resonant point, without sufficient excess angular acceleration, it "locks in" at this roll rate where, from then on, a divergence in the lateral accelerations and rotation rates can be seen. Lastly, the sideslip plot shows a circular motion. This is consistent with the rocket rolling at the resonance frequency [3]. A more detailed explanation is given in subsection C
5.2	Separation System Actuation Actuation of the separation system during powered flight would cause the capsule to separate and the vehicle to become unstable.	Closed	Not available.	If the separation system had actuated, then the recovery bay would likely not have broken at the nosecone interface as the loads on the section would then have been reduced. Additionally, the recovered data does not show the system being commanded to actuate. Separation of debris from the top of the vehicle is also not seen in any form of footage or data.
5.3	Engine Burn Through An engine burn through can cause sideways thrust, causing the rocket to become unstable.	Closed	During ground tests the engine was seen to be prone to burning through.	The recovered engine does not show any sign of burn through.

C. Root cause analysis conclusion: Inertial Roll Coupling

The primary cause of the Stratos III in flight anomaly is concluded to be inertial roll coupling as this is the only failure case that remains open after analysis of the fishbone diagram and eliminating all other failure cause theories.

Inertial roll coupling describes the phenomena where the inertia of a vehicle's fuselage is greater than the aerodynamic stabilising force of the stabilising surfaces of the vehicle. Vehicles like this are susceptible to their roll motion becoming coupled with their pitch and yaw motion. R.E. Day defines it as follows:

"Inertial roll coupling is a resonant divergence in pitch or yaw when roll rate equals the lower of the pitch or yaw natural frequencies" [1]

In practise this means that the rocket body axes starts to precess around the rocket velocity vector and the rocket starts flying in this conical motion. The nose of the rocket is consistently not pointing in the direction the rocket is flying anymore, there is always an angle of attack that keeps increasing over time at a certain rate.

The sideslip plot in Figure 5c clearly shows the circles the angles of attack α and β are going through. This is also consistent with inertial coupling, wherein a rocket makes a coning motion, whilst rolling at the rate of the lateral natural frequency [1, 3].

The most intuitive evidence of inertial coupling can be seen in the animation created from the IMU data, presented in Figure 6. The animation clearly shows that the vehicle's pitch and roll motions are coupled, diverging in behaviour after passing Mach 1, becoming unstable and resulting in disintegration after 22.12 seconds of flight time.

On paper, the clearest source is Figure 10, which is a 3D representation of the orientation of the rocket. It shows the length of the component of the unit vector of the body fixed X axis, resulting from successive projections onto, firstly the world-fixed XY plane and secondly the world-fixed X or Y axis. The plot demonstrates that while the rocket is spiralling due to rotation around its Y and Z axes, it is also rotating around its longitudinal X axis. Note that all of the Y axis vectors face outward from the centre of the spiral, so the same side of the rocket was always facing the velocity vector. This means that the roll rate of the rocket matched the natural pitch and yaw frequencies.

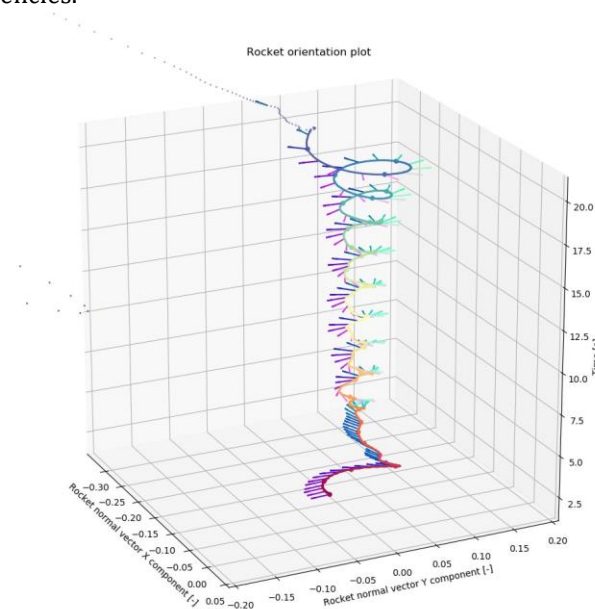


Figure 10: Orientation of the Stratos III rocket during flight, plotted over altitude.

However, the exact cause of a rocket's inertial roll coupling is very difficult to pinpoint as multiple factors play a role in this phenomenon. These factors may be categorised into three main areas; high L/D ratios; an induced aerodynamic pitch moment; and a variety of misalignments all resulting in an effective thrust misalignment. This division is reflected back in Figure 8 where 16 different potential causes are all linked to either or both a significant effective aerodynamic pitching moment and effective thrust misalignments being too large. This division is particularly useful as it is commonly used in literature and thus helps the team structure their recommendations in the following chapter.

VI. Investigation Results

From a critical review of the Stratos III design, numerous aspects can be found that could be adjusted to improve the sections and interfaces of the rocket that are considered to contribute to the inertial coupling motion. These improvements are possible to implement to a certain extent; however, it is beyond the realm of possibility for a student team to acquire the accuracy necessary to completely eliminate these aspects. Even if all the small angles, deflections and the stiffness of the multitude of interfaces could be measured, it would not guarantee success of the next launch as there are likely still small offsets present that a student team would be unaware of and could give rise to the same problems. Large spin-balance facilities would be required to test the rocket and extensive 6 degree of freedom, non-rigid body simulations would need to be performed. These are all outside of the scope of the Stratos project, especially in the time span of a one-year project. Another approach would be to simply launch, observe what happens, modify some part of the design and launch again. This iterative process of trial and error can be very successfully employed for commercial applications, where a large budget is available for the development of a launcher that can be (mass)produced after a successful design is found. For DARE, however, funds are limited, and our vehicles are always experimental. There is no large-scale commercial application, since DARE is a non-profit student society, not a company. This means that other means need to be found in order to assure a successful launch of the next experimental student rocket. These means for combating inertial roll coupling are presented in subsection A and subsection B by following two different approaches of rocket balancing (passive) and rocket control (active).

A. Rocket Balancing

A very effective course of action is to make design recommendations based on research and investigations of similar sounding rockets that have also suffered from inertial roll coupling. Some of these sources are presented in the next few paragraphs, while also highlighting several aspects that are known to easily induce inertial coupling.

1. L/D Effects

Sounding rockets all have a relatively large L/D (length over diameter ratio) compared to larger rockets (Falcon 9 L/D = 18.9, Stratos III L/D = 28.5). This makes sounding rockets naturally prone to the inertial coupling motion. A measure of how likely the rocket is to lock in the inertial coupling motion is the coupling inertia ratio, defined in Equation 1 [1].

$$\frac{I_{xx} - I_{yy}}{I_{zz}} \quad (1)$$

Some ratios for relatively fast and slender aircraft are given in Table 7 [1]. These aircraft are susceptible to inertial roll coupling and some have experienced it to the extent of catastrophic failure. To achieve an estimation of the inertial coupling ratio of the Stratos III rocket, one can assume the rocket to be either a solid cylinder, or a cylindrical shell. These two objects both have very well-defined inertial coupling ratio, which can be plotted as a function of the length to diameter ratio. A rocket with a certain L/D will then be located at some arbitrary point between the two lines. This is shown in Figure 11.

Aircraft	Coupling Inertia Ratio
X-15	-0.94
X-3	-0.88
Shuttle	-0.84
YF-102	-0.81
F-100A	-0.71
X-2	-0.70

Table 7: Primary coupling inertia ratios for various aircraft [1]

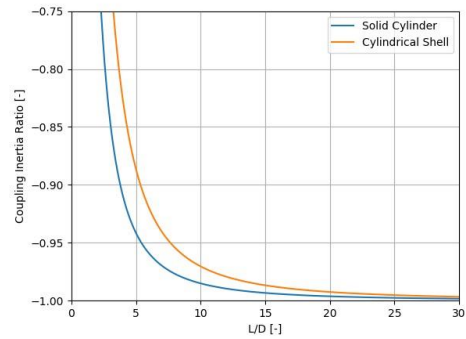


Figure 11: Relationship between coupling inertia ratio and length over diameter ratio. [4]

The closer the coupling inertia ratio lies to -1.0, the more susceptible the vehicle will be to lock into the inertial coupling ratio [1]. Since the L/D of the Stratos III is around 28.5, one can easily determine that the Stratos III rocket is very susceptible to this motion. However, it can also be seen that the L/D of the rocket essentially has to be below 15 before any minor improvement in the coupling inertia ratio can be observed. Since it is very unlikely that DARE will ever develop a rocket with an L/D of lower than 15 due to manufacturing difficulties (manufacturing large diameter parts, above 30 cm, is difficult with the machining capabilities available to DARE), lowering the L/D is not a realistic option for preventing the inertial coupling motion. Moreover, with a lower L/D for a rocket with the same volume, the frontal area would significantly increase. The drag would then scale linearly with the frontal area. This is exactly the reason why sounding rockets still have this large L/D and all of them deal with inertial roll coupling in a different manner.

2. Rocket Body Flexibility and Misalignments

Flexibility of the rocket body and inherent misalignments in the assembled rocket are a big contributing factor to the inertial coupling motion. This subsection summarises the results of multiple papers that provide recommendations about the rocket structural design.

The first investigation is on the dynamic stability of sounding rockets [5]. This paper presents research on the effects of joint rotation and compliance, body flexibility, fin flexibility, and induced and non-linear aerodynamic characteristics on roll resonance behaviour. The most important conclusions are noted:

- *Joint rotation can provide a major source for roll lock-in.*

The Aerobee 150 flight 4.81 failed due to roll lock-in. It was known to have an extreme amount of 12 joints (interfaces). Therefore, the rocket was very susceptible to roll lock-in. Also, it is mentioned that the primary cause for failure of flights 4.81 and 4.86 is the joint play. This indicates that the joints were not rigid enough.

- *Joint compliance and vehicle bending yield minor increase in aerodynamic trim, but a major increase of thrust misalignment.*

This means that the flexibility of the rocket is not a major problem for the aerodynamics of the rocket, but it is for the thrust misalignment.

The second paper is based on the Aerobee 150 flights [6]. The Aerobee 150 is a two-stage sounding rocket from NASA, the first stage being a solid booster, and the second a liquid propelled sustainer [6]. The Aerobee 150 parameters can be found in Table 8. The Aerobee 150 launched 453 times between 1959 and 1983 [7]. On the 9th of April 1964 and the 14th of April 1964, flights NASA 4.81 GG and NASA 4.86 NA successively malfunctioned due to what appeared to be inertial coupling. Those flights are compared to flights NASA 4.15 GG and NASA 4.88 GT, which have a similar configuration but did launch successfully. The primary cause of the malfunctions of flights 4.81 GG and 4.86 NA was structural and aerodynamic yaw coupling. To avoid similar failures, the following recommendations were made.

- Carry out more precise alignment checks.

The final fin and thrust chamber alignment checks shall be performed after the rocket tail-can has been installed the final time, making the measurements as representative of flight conditions as possible.

- More thorough assembly instructions.

More thorough instructions for (payload) assembly, including torqueing procedures for rocket screw joints and payload alignment, have been provided for the rocket preparation personnel.

- Proper preflight checks.

Preflight checks and preparations have been revised, updated and are strictly monitored by the vehicle manager responsible for the flight.

- Finally, the engineers came up with limiting conditions for Aerobee 150 flights:

- The static margin, defined by $\frac{|x_{cp}| - |x_{cg}|}{d}$, shall be greater than 2. Here x_{cp} is the position of the centre of pressure in the rocket body frame, x_{cg} is the position of the centre of gravity in the rocket body frame and d is the diameter of the rocket,
- Roll rate at burnout shall be between 2 and 3 rps.
- The misalignment of the thrust chamber shall be maximum 5.1 mm.

Since the Aerobee 150 is very similar to the Stratos III rocket, it is assumed that similar constraints apply.

The third paper presents sources that cause roll lock-in in sounding rockets [3]. It is especially focused on the Aerobee 150A, which is almost exactly similar to the Aerobee 150, the biggest difference being that the 150A has 4 fins and the 150 only 3.

Disturbance sources, the inevitable asymmetries resulting from manufacturing and assembly tolerances, fin adjustment, measurement inaccuracies, and random flight environment uncertainties, can be classified conveniently into three principal categories: configuration, mass distribution, and aerodynamic-geometric interactions. Configuration asymmetries cause an effective change in fin cant δ and/or a static trim angle of attack α_{ST} through an aerodynamic moment or thrust moment. Mass asymmetries change the static stability margin and α_{ST} , cause rotation of the axes of the principal moments of inertia and provide roll coupling with the aerodynamic normal force. Aerodynamic-geometric interactions cause induced roll and aeroelastic bending.

Evaluation of the Δcg tolerance for an appropriate range of C_{m0} and τ yields the asymmetry tolerance contours shown in Figure 12 for the Aerobee 150A vehicle. Below and left of the contour the asymmetry tolerances will not cause lock-in.

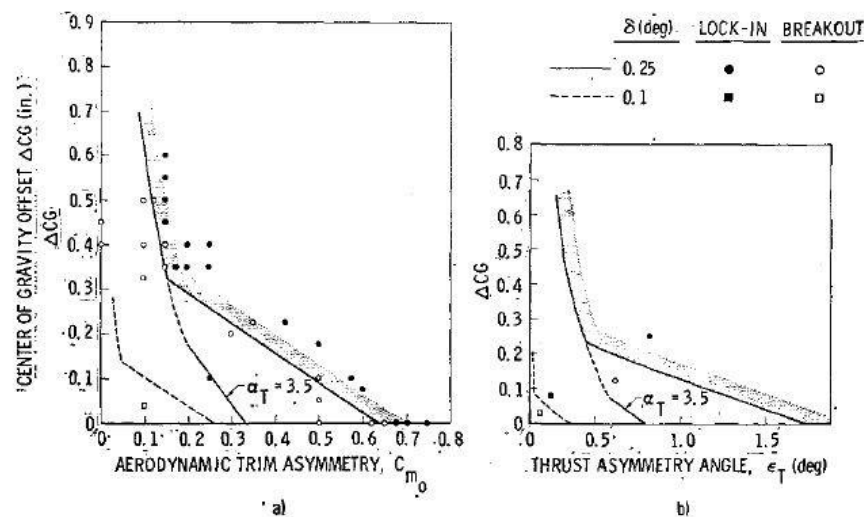


Figure 12: Centre of gravity asymmetry tolerances for the Aerobee 150A vehicle [3]

For their nominal $\delta = 0.25^\circ$ they find the contours contain reasonable asymmetry tolerances. The tolerable Δcg offset increases significantly as c_{m0} and τ decrease. A drastic decrease in tolerances occurs if δ is reduced to 0.1° , due to an increase of the altitude at which resonance occurs. For a student project, the tolerances at a nominal effective fin cant are already hard to realise, but the additional uncertainty due to vehicle differences and altitude sensitivity even more emphasise how hard it is to predict rocket dynamic stability before any validation launch.

The fourth paper explains the development of the Aerobee 350 rocket [8, 9], of which the specifications can also be found in Table 8. The authors reach the following conclusions:

- *Thrust misalignment threshold.*

To prevent lock-in into the inertial coupling motion, the thrust misalignment shall be lower than $1.60^\circ \cdot 2.0^\circ$. In addition, it was found that the 2.0° thrust misalignment will only cause lock-in at a specific roll orientation.

- *Fin misalignment threshold.*

To prevent lock-in into the inertial coupling motion, the fin misalignment shall be lower than 0.40° to 0.45° .

- *Wind shear.*

Triangular wind shears of 30 and 76 m/s acting from 12.5 to 13 km altitude would not induce lock-in into the inertial coupling motion. Therefore, wind is not a major influence on inertial coupling lock-in.

Table 8: Specifications of Aerobee 150, 350 and Stratos III [7, 9]

Specification/Rocket	Aerobee 150 4.81 GG	Aerobee 350	Stratos III
Length [m]	8.5	15.90	8.2
Diameter [m]	0.38	0.56	0.28
L/D	22.4	28.39	29.3
Total mass [kg]	930	2921	344.7
Peak thrust	18 kN	217 kN	26 kN
Stages	2	2	1
Propulsion system	Liquid (solid booster)	Liquid (solid booster)	Hybrid

B. Rocket Control

In order to be able to confidently mitigate the susceptibility to inertial coupling in future DARE rockets, all of the aforementioned improvements and their contributions to inertial coupling need to be quantified. As mentioned before, DARE does not have the resources to perform the analysis, simulations and system tests required to perform this quantification. One method that will provide a guarantee that the rocket will not exhibit inertial coupling, is through ensuring sufficiently high or low roll rates. However, such an active or passive control system is difficult to implement, might require a completely new subsystem to be developed and adds new launch site requirements.

Despite these challenges, the recommendation of the investigation team remains to develop a system to, either actively or passively, control the roll rate of the rocket, as this is the only method that will completely ensure the mitigation of inertial roll coupling. The trade-off and exact determination of this system is left to the Stratos IV team completely.

VII. Conclusion & Recommendations

This section presents the final conclusions of the investigation into the in-flight anomaly of the Stratos III sounding rocket, as well as providing a number of recommendations for the conduction of and preparation for future post-flight analyses and investigations.

A. Root-Cause of Stratos III In-Flight Anomaly

The cause of Stratos III's in-flight anomaly is determined to be a motion called inertial coupling, defined as when a vehicle's roll motion becomes coupled with its pitch and yaw motion. When the lower of the pitch or yaw natural frequencies is equal to the roll rate, then the vehicle becomes unstable. Inertial roll coupling in turn has a number of contributing factors, being a large L/D, flexible rocket sections and joints, joint and section misalignment and vehicle balancing. Measurement and rectification of these aspects is one method of mitigating inertial coupling, however this measurement is resource intensive to carry out, and does not guarantee eradication of this phenomena without extensive testing. Active control of the vehicles roll is one method that will assure mitigation of this motion, by maintaining the vehicles roll rate above or below the susceptible rates.

B. Assistance to Future Investigations

There is a twofold lesson to be learnt in order to assist future investigations. Generally, the more data that is acquired about the flight, from both on board and ground sources, the better, but additionally, in order for judgements to be made about the vehicle's behaviour and performance post flight, the vehicles parameters must be known accurately pre-flight.

Regarding in-flight information gathering there are a number of points of recommendation:

- **Ensure functioning of black boxes.** Housekeeping data recorded by the flight computer was not correctly duplicated to the black boxes. This meant that the loss of one of the SD cards on the flight stack led to losing most on-board stored housekeeping data.
- **Log high frequency IMU data to black boxes.** The complete IMU data was only logged to SD cards directly mounted on the PCBs of the flight computer. Loss of any of these SD cards would have considerably complicated failure analysis.
- **Stream back at higher data rates.** It should be investigated what telemetry data rate is required to allow for a proper investigation. One cannot assume that black boxes will be found after an anomaly, as the majority of the flight occurs over the ocean. Thus, enough data should be sent back via telemetry to be able to conduct a proper analysis of a possible anomaly.
- **Ensure functioning of pressure sensors.** The pressure sensors present on the combustion chamber and the oxidiser tank failed to function during the Stratos III operations and flight. This failure makes it difficult to analyse engine performance post flight.
- **Adapt camera to view better in the dark.** The cameras placed on Stratos III provided very little information for the investigation as they provided very limited visibility during the night of the rocket launch.
- **Store camera footage in black boxes.** The cameras on board of Stratos III were outside of the nosecone. If footage recorded by them would have been stored in black boxes inside the nosecone the camera footage could have been retrieved.

Information that should have been recorded accurately pre-flight in order to be available for caparison in a post flight analysis or investigation includes:

- **Record meteorological data.** During the Stratos III final launch procedures, a launch delay of circa 10 hours meant no meteorological balloons had been released recently, and the wind conditions present at the moment of launch were not recorded by the team. This information is critical in a post flight analysis and its recording should be implemented into the launch procedures, within the final hour of the countdown procedures.

- **Deflection of the vehicle sections.** Rigidity of Stratos III's interfaces is considered to be a main source of the inertial coupling motion, however the rigidity of these interfaces was not measured during assembly or before the launch. From personal recollection it is known that these sections visibly flexed when assembled under normal handling loads, however, as this was not measured or recorded it is very difficult to comment concretely on this.
- **Misalignment of vehicle sections.** Similar to the deflection, misalignment of vehicle sections is considered to be a main source of the inertial coupling motion, however the misalignment of these sections was not measured during assembly or before the launch.
- **Final dimensions of the vehicle.** The final dimensions of the vehicle were not recorded. Adjustments made between the CAD model and actual produced vehicle were not recorded in a systematic manner.
- **Section masses of the vehicle.** Similar to the dimensions, the mass of different vehicle sections was not recorded during construction and assembly.
- **Wet mass of the vehicle upon take-off.** Due to a malfunction in the load cell measurement of the complete vehicle during oxidiser filling, the final loaded oxidiser mass was estimated from thermal camera footage and the fact that it was visually confirmed that the dip tube of the tank had been reached. This oxidiser mass is critical for any form of post flight analysis.
- **General observations during assembly.** Any deviation from the intended assembly process or configuration should be recorded in the event that this deviation may be linked to an in-flight failure (eg. an interface failure).
- **Conduct a wet dress rehearsal pre-flight.** A wet dress rehearsal with loaded fuel and oxidiser should be conducted in order to identify issues such as the load cell malfunction during filling. In this test all of the electronic systems and all of the interfacing with them can also be tested.
- **Conduct a mock flight investigation pre-flight.** A flight investigation should be performed after a dress rehearsal to ensure functionality of all recording and telemetry systems.
- **Conduct fin bending tests.** Rigidity of the fins is a crucial parameter in ensuring aerodynamic stability. This test was not performed for the flight version of the Stratos III fins and it is recommended that this absolutely be performed in the future, especially when last minute changes need to be made.
- **Prevent implementation of untested adjustments to the vehicle design.** In line with the fact that the final design, masses and dimensions were not recorded, in the case that adjustments are necessary between the final design and launched version, these should be avoided unless absolutely necessary, and if so, should be recorded well.
- **Accurately record the complete attitude of the filled rocket in the tower.** The azimuth and pitch of the initial rocket orientation were recorded accurately when the tanks were empty. Comparison of the measured rocket trajectory with radar data suggests that the actual angles were different.

With regards to the composition of an investigation team and their conduction of a post flight analysis or investigation, the driving force behind the completion of the Stratos III investigation, was the necessity of mitigating the failure in Stratos IV. Thus, the majority of the investigation team were members of Stratos IV and there was very little involvement of members of Stratos III. This meant that members were more impartial when conducting the investigation but were impeded by their limited knowledge of the rocket and the launch campaign. It also meant that members were motivated to complete the investigation in order to obtain the results for the Stratos IV rocket. This meant that when the initial results that had implications for the Stratos IV rocket were found, then the momentum behind the investigation stalled. This result driven focus meant that the completeness of the investigation was limited, and the motivation to document, occasionally, lacking. This could perhaps be assisted in future by planning before a launch campaign who will take part in a post flight analysis/investigation and set intermediary and final deadlines for this analysis.

Acknowledgements

The authors would like to extend their thanks to a number of parties for their assistance and advice in the completion of this investigation and paper. From the Delft University of Technology ir. Michiel Schuurman, ir. Barry Zandbergen, and ir. Marc Naaije provided advice on the conduction of an aerospace focused investigation. The members of INTA at the CEDEA launch site assisted in the conduction of the launch campaign and provided the recorded ground data to the investigation team.

References

- [1] Day, R. E., *Coupling Dynamics in Aircraft: A Historical Perspective*, Dryden Flight Research Center Edwards, California, 1997.
- [2] Murphy, C. H., "Some special Cases of Spin-Yaw Lock-In," Tech. rep., US army ballistic research laboratory, 1987.
- [3] Jr., D. P., "Sources, Mechanisms, and Control of Roll Resonance Phenomena for Sounding Rockets," *Spacecraft*, Vol. 4, AIAA, November 1967, p. 1521.
- [4] Nakka, R., "Launch Report – Frostfire One Rocket," 2003.
- [5] Jr, D. P. and Woods, P., "Final Report for Dynamic Stability Study for Sounding Rockets," Tech. rep., Lockheed Missiles and Space Company, 1968.
- [6] Busse, J. R. and Kraft, G. E., "Aerobee 150 Structural and Aerodynamic Pitch Coupling," Tech. rep., Goddard Space Flight Center, 1966.
- [7] Astronautix, "Aerobee 150," 2017, <http://www.astronautix.com/a/aerobee150.html>.
- [8] Lane, J. and Chalfant, C., "Development of the Aerobee 350 Sounding Rocket," *Sounding Rocket Vehicle Technology Specialist Conference*, AIAA, June 1967, p. 47.
- [9] Astronautix, "Aerobee 350," N/A, <http://www.astronautix.com/a/aerobee350.html>.

Appendix A. Implementation in Stratos IV

As mentioned in this paper, the largest drive to complete the investigation was the need of a conclusion in order to implement appropriate changes to the Stratos IV rocket and prevent a similar failure. The initial timeline was to launch to space during the summer of 2019, one year after the launch of Stratos III. This pressing timeline caused the investigation to be performed during the design of the Stratos IV rocket. The implementation of the recommendations from this investigation happened during the investigation itself. This appendix aims to show what was done for Stratos IV to give a more complete picture of what this investigation yielded in the end.

One of the most important focus points was the structural rigidity of the rocket, and especially the interfaces. This was also the case because the observations of the rocket before launch already indicated that the rigidity of the rocket was not optimal. Moreover, the offset of the centre of gravity and moment of inertia is something that is taken into account.

To increase the structural stiffness of the rocket, a design requirement of a maximum deflection of the engine compared to the centre line of 5.1 mm was set [6]. This is the total deflection caused by misalignment of the different parts, as well as the flexibility in the structure itself. The carbon fibre combustion chamber is designed to not deflect more than 1 mm with the maximum fin loads of 4000 N, applied at approximately 75% of the chamber length.

Furthermore, the interfaces were redesigned such that bolts are never used for alignment of the rocket parts, which was the case in Stratos III, where the radial bolts holding the injector in place inside the combustion chamber were simultaneously the sole connection between the engine casing and the rest of the rocket. It was decided to use faces of parts for alignment, while still using bolts for attachment. This can be done by using a conical interface. A concept drawing of this is shown in Figure 13. Since the flatness tolerance on these parts can easily be within ± 0.05 mm, the resulting misalignment angle is significantly reduced.

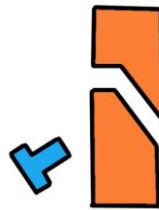


Figure 13: Conical interface concept

By designing more rigid alignment jigs, which at the same time allow for the to be attached parts to be shimmed into the correct position, the misalignment angle in glued interfaces is also significantly reduced. This way, laser alignment can be used instead of trusting the rigidity and accuracy of the jig. This makes alignment within 0.05° possible.

By paying attention to centre of gravity location in the design phase, the imbalance in the rocket during flight can be reduced. Since DARE does not have access to spin-tables, it is very hard to determine the centre of gravity and the moment of inertia of the various rocket parts. This is why these variables are determined using the 3D modelling software, CATIA V6, that is used to design the rocket. By modelling all of the components, weighing them after production and overwriting the mass calculated by CATIA, a reasonably accurate number for the centre of gravity and the moment of inertia can be determined.

To increase the aerodynamic stability of the rocket, two design changes were implemented. First, the shape of the fins was changed. It was discovered that for stable flight, the static margin shall be higher than 2[6]. For the Stratos III rocket, this would not have been the case at higher altitude, so it had a higher chance of becoming unstable in the part of the flight after the anomaly. With the new fin design, the static margin over time curve is flattened, while still keeping it above 2 at all times. Because of the lower static margin at the start of the flight, the rocket will be less prone to wind cocking. A plot of the static margin can be seen in Figure 14.

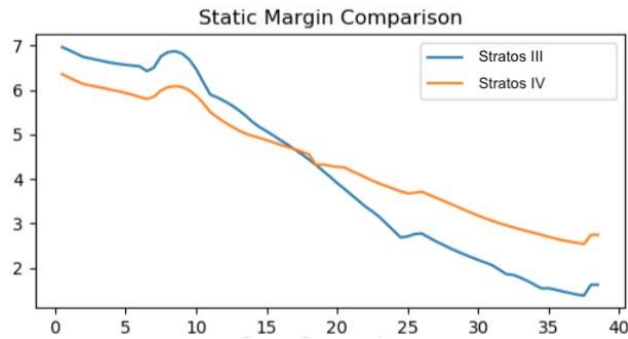


Figure 14: Static margin over time

Secondly, an active roll control system is introduced. This system uses the same nitrous oxide as the main engine, but runs it over a ZrO_2 catalyst foam bed coated with NiO and heated by heating wire to a temperature of approximately $600\text{ }^\circ\text{C}$. In a stainless-steel 3D printed combustion chamber, the nitrous oxide decomposes and produces approximately 40 N of thrust. Four of these thrusters are placed along the skin of the rocket and intend to keep the rocket's roll rate within reasonable bounds. It was decided to not implement spin stabilisation, since the required roll rate, as well as the required fin cant to achieve a specific roll rate are unknown and very hard to test. Moreover, it is unclear how the large spin rate would affect the liquid oxidiser in the tank, and as such also the engine performance.

Since DARE does not have access to a 3-axis thrust measurement bench, and designing one was, after analysis, determined to be too hard, the thrust misalignment of the engine will be unknown. This will be a risk during launch.

Due to lack of time, and the delay of the investigation, no time could be spent on the design of a different telemetry system with a sufficient data rate to perform an investigation without recovery of the black boxes. It is recommended this is implemented before the launch of Stratos IV.